Chemical order and magnetic behavior of Fe-dilute fcc Fe-Pd nanoparticles

R. A. Guirado-López,[1,2,*] M. C. Desjonquères,[1,†] and D. Spanjaard[3,‡]
[1]*Commissariat ý l'Energie Atomique, DSM/DRECAM/SPCSI, Centre d'Etudes de Saclay, F-91191 Gif-sur-Yvette, France*
[2]*Instituto de Física "Manuel Sandoval Vallarta," Universidad Autónoma de San Luis Potosí, Alvaro Obregón 64, 78000 San Luis Potosí, Mexico*
[3]*Laboratoire de Physique des Solides, Bâtiment 510, Université Paris-Sud, Centre d'Orsay, 91405 Orsay, France*
(Received 8 February 2006; revised manuscript received 5 July 2006; published 16 August 2006)

The chemical order and magnetic behavior of Fe-dilute fcc Fe-Pd nanoparticles are theoretically investigated using many-body potentials derived in the framework of the generalized second moment approximation (SMA) and self-consistent spin-polarized tight-binding electronic structure calculations, respectively. The SMA total energy calculations reveal that surface sites and the core region are not favorable positions for the Fe impurities and that they prefer to accumulate in the subsurface region of the particles, showing a very strong tendency to separate. However, additional contrasting atomic configurations close in energy are also found which could imply the coexistence in real samples of several Fe-Pd nanoparticles with a well-defined composition, but having different chemical orderings. Magnetic properties are first investigated for a single Fe impurity in bulk Pd, allowing an extension of the polarization cloud around the Fe atom much larger than in an *ab initio* calculation. The results are in good agreement with experiments and serve as a reference to identify surface and size effects in FePd nanoparticles. Nanoparticles containing from 135 to 561 atoms with up to three Fe substitutional impurities are then investigated, as well as more concentrated ($\simeq$10% Fe content) shell structures. The extension and magnetic structure of the Fe-induced polarization cloud is studied in detail as a function of the size, surface termination, and the precise location and number of the iron impurities in the particles. The local electronic structure at the Pd sites located at the outermost atomic shell is considerably perturbed by the subsurface position of the Fe atoms and could modify the catalytic properties of palladium nanoparticles. Finally, we show that the value of the orbital-to-spin ratio in our Fe-Pd clusters is very sensitive to the changes in the internal position of the Fe impurities, a result that suggests that x-ray magnetic circular dichroism experiments can be very useful in order to reveal precise features of the chemical order in these magnetic nanoparticles.

DOI: 10.1103/PhysRevB.74.064415 PACS number(s): 75.75.+a, 75.25.+z, 61.46.Bc, 73.21.−b

I. INTRODUCTION

It is well known that solids made of 4*d* elements are nonmagnetic. However, it has been clearly established that the late 4*d* elements should exhibit a magnetic moment when their atomic volume[1–3] is moderately increased or, possibly, in clusters (Rh, for instance).[4] In addition, the presence of a 3*d* ferromagnetic impurity (Fe, Co, or Ni) induces a spin polarization in its vicinity.[5,6] In particular, much experimental interest has been directed to analyze the magnetic properties of Fe-Pd compounds in the form of bulk alloys,[7,8] thin films,[9,10] and multilayered structures.[11] In the previous examples, both Fe and Pd species are placed in contrasting local atomic environments in which Fe atoms can be found as isolated impurities or highly interacting species in a bulk Pd host, as well as defining complex FePd surfaces or interfaces with different degrees of intermixing. Despite the remarkable variations in the structure and dimensionality of these systems, general trends concerning the magnetic behavior of the Fe atoms and the magnetic response of the Pd sites can be established from experimental data, namely (i) both spin and orbital moments at the Fe sites are generally enhanced with respect to their bulk values; (ii) Fe atoms tend to polarize adjacent Pd sites leading to the formation of giant moments or polarization clouds that extend, for example, over a range about 10 Å around a single Fe atom in dilute bulk alloys (implying a rapid variation of the induced moment with the concentration due to interference effects), or to a depth of about 20 Å from the FePd interface in Fe/Pd multilayers; (iii) the Pd polarization is highly temperature dependent; (iv) the local moments at both Fe and Pd sites most often couple ferromagnetically (although there is some evidence also of antiferromagnetic coupling), and (v) there is a strong correlation between the magnetic properties and the degree of chemical order in the samples.

From the theoretical side, Fe-Pd bulk alloys with different compositions, as well as various low-dimensional structures, have been extensively analyzed by means of different approaches.[6,12–14] These studies include the magnetic behavior of isolated Fe atoms embedded (deposited) on Pd bulk (surfaces), the magnetic properties of ultrathin Pd films grown on Fe substrates (or vice versa), and Fe/Pd multilayered structures with varying thickness and composition. From these investigations it has been found that the strong hybridization between the Fe-3*d* and Pd-4*d* bands plays a crucial role in determining the electronic and magnetic properties of the materials. These hybridization effects lead to the formation of local magnetic moments in well-defined regions of the structures called polarization clouds. Obviously, those palladium atoms located far away from the Fe species will be little affected by the inclusion of the magnetic impurities. It is clear then that both electronic and local environment effects determine the extension of the Fe-induced polarization clouds, as well as the precise details of the local moment distribution.

In spite of the above extensive investigations, the magnetic properties and atomic ordering processes of Fe-Pd alloys in the form of isolated clusters or nanoparticle arrays have not received similar attention. These kinds of nanostructures are also of fundamental importance due to their possible applications as magnetic recording media or to their use as novel catalytic materials. On the one hand, theoretical calculations, mostly within the framework of density functional theory (DFT), have been performed for relatively small Pd clusters having up to 55 atoms in which a single Fe atom was always included as a substitutional impurity in the center of the particles.[15] In general, the main motivation of these studies was to try to understand the magnetic behavior of Fe impurities in bulk Pd by using a cluster model for the macroscopic alloy. In fact, these calculations reproduce the main experimental features of dilute samples, showing a modest induced magnetic polarization on neighboring Pd host atoms, which decays with distance from the Fe impurity.

From the experimental side, and due to the recent advances in gas evaporation and sputtering methods, as well as in chemical synthesis techniques, a wide variety of Fe-Pd nanoparticles with different sizes, morphologies, and compositions can be now currently made. The experimental characterization of these systems has revealed the existence of interesting complex phenomena that includes fcc to fct (face-centered tetragonal) structural transformations,[16] strong changes in the coercivity with annealing of the samples,[17] as well as a highly dependent saturation magnetization on the particle size and composition.[18,19] In general, strong finite-size effects are expected in Fe-Pd nanoparticles and it is clear that the form and extension of the Fe-induced polarization clouds will be considerably influenced by the size of the Pd host, as well as by the strong localization effects present at the cluster surface. Furthermore, even in dilute Fe-Pd alloys, a Fe impurity will possibly have another Fe impurity as its nearest or next nearest neighbor, inducing the appearance of Fe-Fe hybridization effects and of strongly interfering polarization clouds.

In this paper we present a systematic theoretical investigation of the chemical order and magnetic properties of Fe-dilute Fe-Pd cluster alloys. We follow a hybrid approach combining two different models. On the one hand, the most favorable positions of Fe atoms in the considered Pd nanoparticles are determined by minimizing the total energy of the cluster alloys, calculated using a many-body semiempirical potential derived in the framework of the generalized second moment approximation (GSMA). On the other hand, we study the magnetic properties using a self-consistent spin-polarized tight-binding model. The case of a single Fe impurity in bulk Pd is first investigated to verify that this model gives results in good agreement with existing *ab initio* calculations and to serve as a reference to put forward the size and surface effects present in clusters. Then we study the lowest energy chemical orderings found for FePd clusters. Specifically, and guided by x-ray diffraction patterns[16,19] and Mossbauer spectroscopy experiments[20] obtained from agglomerates of Fe-Pd nanoparticles, we consider only compact fcc cluster arrangements. The efficiency of both approaches allows applications to cluster sizes well beyond the range of *ab initio* techniques. We focus on the dependence of the magnetic properties on relevant variables, such as Fe-impurity content, surface structure, and particle size. Finally, by calculating the orbital magnetic moment to spin magnetic moment ratio for different cluster alloys, we show that the use of x-ray magnetic circular dichroism experiments can be very useful in order to reveal precise features of the chemical order within magnetic nanoparticles. The paper is organized as follows. In Sec. II we describe the theoretical models used for the determination of the lowest energy atomic configurations, as well as for the calculation of the electronic and magnetic properties of the systems. Section III is devoted to the study of a single Fe impurity in bulk Pd. In Sec. IV our results for FePd clusters are discussed, and finally in Sec. V the summary and conclusions are given.

II. THEORETICAL MODELS

Structural and electronic aspects have to be considered in the study of the magnetic properties of Fe-Pd cluster alloys. Strictly speaking, calculations involving a simultaneous unconstrained relaxation of the geometry and unrestricted total spin value for the clusters are necessary. However, these types of calculations imply formidable computational requirements. Actually, for clusters containing more than seven atoms, the *ab initio* determinations of the ground-state atomic structures become computationally difficult and, already for that range of sizes, it is common to combine different theoretical approaches to obtain, first, the ground state atomic structures within a simplified scheme (semiempirical potentials, absence of magnetic interactions, etc.), and then use a high level of theory to analyze the electronic and magnetic properties of the systems. In this paper we follow the same methodology and start with a brief description of the models.

A. The semiempirical many-body potential

In order to find the optimal positions of the Fe atoms inside the clusters, we have set up an alloy potential which is the sum of a repulsive pairwise contribution and an N-body attractive term

$$E_{tot} = \sum_i E_i = \sum_i \left(\sum_j A_{ij} \exp\left[-p_{ij}\left(\frac{r_{ij}}{r_{0ij}} - 1 \right) \right] - \left\{ \sum_j \xi_{ij}^{1/\alpha} \exp\left[-2q_{ij}\left(\frac{r_{ij}}{r_{0ij}} - 1 \right) \right] \right\}^{\alpha} \right). \quad (1)$$

r_{ij} is the distance between two lattice sites i and j which are occupied either by an Fe or by a Pd atom, in practice interactions are cut-off when r_{ij} exceeds the next nearest neighbor (NNN) distance. A_{ij}, p_{ij}, ξ_{ij}, and q_{ij} are parameters which can take three values depending on the nature of the bond ij (Pd-Pd, Fe-Fe, or Pd-Fe) and r_{0ij} are reference distances corresponding to the three types of bonds. Finally the exponent α describes the many-body nature of the potential and should be strictly smaller than 1. This condition on α has a clear physical origin; the energy E_i of an atom i should decrease more and more slowly when its coordination increases towards the bulk coordination. In the so-called second moment

TABLE I. The parameters defining the potential of Pd-Fe alloys: A_{ij} and ξ_{ij} are given in eV and r_{0ij} in Å.

Atom pair	A_{ij}	p_{ij}	ξ_{ij}	q_{ij}	r_{0ij}
Pd-Pd	0.142	11.55	1.054	2.53	2.750
Fe-Fe	0.184	8.59	1.293	1.68	2.481
Fe-Pd	0.181	10.07	1.307	2.11	2.616

approximation (SMA), which has often been used in the literature, $\alpha=1/2$. However, it has been suggested[21] that using $\alpha=2/3$ would be more appropriate to take into account the influence of higher order moments and actually improves significantly the numerical values of the surface energies.[22] Thus all our calculations have been carried out with $\alpha=2/3$. The parameters relative to a bond between two atoms of the same chemical species have been fitted from a number of physical quantities, the reference distance r_{0ij} being the bulk equilibrium nearest neighbor (NN) spacing which should obey the bulk equilibrium equation. The chosen physical properties include the experimental cohesive energy and bulk modulus, as well as the surface energies of the three low index surfaces [(111),(100),(110)] taken from *ab initio* calculations.[23] Indeed, in small clusters the proportion of surface atoms is large and it is important that the potential describes fairly accurately the surface energetics. We have verified that the elastic constants C and C' are in qualitative agreement with experimental values. The Fe-Fe and Pd-Pd parameters are given in Table I and the fitted physical quantities are compared to the fitting database in Table II.

The parameters corresponding to heteroatomic bonds can be obtained using a fit on already known properties of ordered alloys. Since in this work we only consider Pd clusters with a low Fe content, we have restricted ourselves to the alloys Pd_3Fe and PdFe for which the equilibrium lattice parameter, formation energy, and bulk modulus are known from *ab initio* calculations.[12] Taking $r_{0ab}=(r_{0aa}+r_{0bb})/2$ as the reference distance, it is often assumed in the literature that the parameters for heteroatomic bonds are given by $p_{ab}=(p_{aa}+p_{bb})/2$, $q_{ab}=(q_{aa}+q_{bb})/2$, $A_{ab}=(A_{aa}A_{bb})^{1/2}$, $\xi_{ab}=(\xi_{aa}\xi_{bb})^{1/2}$. We have used these expressions as starting points but we have allowed all of them to vary by several percent. Finally, a very good agreement was found by increasing the above values of A_{ab} and ξ_{ab} by 12%. The resulting parameters for heteroatomic bonds are given in Table I and the fitted properties of the two ordered alloys are compared to the *ab initio* calculations of Kuhnen and da Silva[12] in Table III. As we can see, the good agreement between our theoretical data and more elaborated calculations is very satisfactory and will serve as a basis to accurately describe the chemical ordering in our considered Fe-dilute Fe-Pd nanoparticles.

TABLE II. The fitted values of the cohesive energies (E_{coh} in eV/atom) bulk moduli (B in GPa) and of the surface energies (in eV/surface atom) of the three low index surfaces of Pd(fcc) and Fe(bcc) compared with the fitted data (the experimental values of B and the surface energies obtained from the *ab initio* calculations have been obtained from Ref. 23).

Element	E_{coh}	B	$E_S(111)$	$E_S(100)$	$E_S(110)$
Pd (fit)	4.03	194	0.63	0.79	1.24
Pd (data)	3.89	195	0.68	0.89	1.33
Fe (fit)	4.85	152	2.34	1.29	0.81
Fe (data)	4.35	168	2.69	1.27	0.98

TABLE III. The fitted values of the lattice parameters (a in Å), the formation energies (E_{form} in eV/atom) and of the bulk moduli (B in GPa) of Pd_3Fe and PdFe ordered alloys compared with the fitted data drawn from the *ab initio* calculations by Kuhnen and da Silva (Ref. 12).

Alloy	a	E_{form}	B
Pd_3Fe (fit)	3.82	−0.20	207
Pd_3Fe (data)	3.86	−0.18	183
PdFe (fit)	3.75	−0.27	204
PdFe (data)	3.78	−0.28	215

B. Tight-binding electronic Hamiltonian

The next step is to apply a self-consistent tight-binding approach to analyze the electronic and magnetic properties. The electronic Hamiltonian includes the intra-atomic Coulomb interactions treated in the unrestricted Hartree-Fock approximation. The model has been described in detail elsewhere;[24] thus, we only summarize its main points and discuss the choice of parameters. In the usual notation the Hamiltonian is given by

$$H=\sum_{i\lambda,\sigma}\Delta\epsilon_{i\sigma}n_{i\lambda\sigma}+\sum_{i\lambda,j\mu,i\neq j,\sigma}t_{i\lambda,j\mu}c^{+}_{i\lambda\sigma}c_{j\mu\sigma}, \tag{2}$$

where $c^{+}_{i\lambda\sigma}$ ($c_{i\lambda\sigma}$) refers to the creation (annihilation) operator of an electron with spin σ in the d orbital, λ at atomic site i, and $n_{i\lambda\sigma}=c^{+}_{i\lambda\sigma}c_{i\lambda\sigma}$ defines the electron number operator. The first term of Eq. (3), $\Delta\epsilon_{i\sigma}$ corresponds to the site- and spin-dependent energy shift of the d level $\epsilon_{i\sigma}=\epsilon^{0}_{d}+\Delta\epsilon_{i\sigma}$ (where ϵ^{0}_{d} stands for the d orbital energy in the nonmagnetic bulk which has been taken as the energy zero) and is determined by the global charge $\Delta n(i)$ and the spin $S(i)$ as follows:

$$\Delta\epsilon_{i\sigma}=U(i)\Delta n(i)-\sigma J(i)S(i), \tag{3}$$

[$\sigma=+1$ (-1) for spin up (down)] with $\Delta n(i)=n(i)-n_d$(bulk). The average intra-atomic direct Coulomb repulsion integral is denoted by $U(i)$ and the average exchange integral is denoted by $J(i)$. They depend on the chemical species of the atom located at site i. In the second term of Eq. (3), $t_{i\lambda,j\mu}$ denotes the corresponding hopping integrals between atoms at sites i and j and orbitals λ and μ. The number of d electrons at site i,

$$n(i)=\sum_{\lambda}(\langle n_{i\lambda\uparrow}\rangle+\langle n_{i\lambda\downarrow}\rangle), \tag{4}$$

and the local spin $S(i)$ at each cluster site i,

$$S(i) = \frac{1}{2}\sum_{\lambda} (\langle n_{i\lambda\uparrow}\rangle - \langle n_{i\lambda\downarrow}\rangle), \tag{5}$$

are calculated self-consistently by integrating the local density of states (LDOS) $\rho_{i\lambda\sigma}(\varepsilon) = -(1/\pi)\mathrm{Im}\{G_{i\lambda\sigma,i\lambda\sigma}(\varepsilon)\}$ (where $G(\varepsilon) = [\varepsilon - H]^{-1}$ is the Green function operator) up to the Fermi level ε_F which is determined by the total number of d electrons in the clusters. The LDOS $\rho_{i\lambda\sigma}(\varepsilon)$ are computed by using the Haydock-Heine-Kelly's recursion method[25] in which $G_{i\lambda\sigma,i\lambda\sigma}(\varepsilon)$ is written as a continued fraction. For systems with an infinite number of atoms the continued fraction coefficients are calculated exactly up to a given number N_l of levels (i.e., the first $2N_l$ moments of the LDOS are exact) and then terminated with the usual square root terminator. In the case of clusters the number of levels of the continued fraction is finite, the recursion process stops at N_l' steps and thus the result for $\rho_{i\lambda\sigma}(\varepsilon)$ corresponds to the exact solution of the single-particle problem.

The parameters used for the calculations concerning a Fe impurity in bulk Pd and Fe-Pd cluster alloys are the following. The two-center d electron hopping integrals (σ, π, δ) between atoms of the same element (i.e., Fe-Fe and Pd-Pd) are taken proportional to $(-6, 4, -1)$ (Ref. 26) and fitted to reproduce the bulk d-band widths of the elements involved,[27] namely, $W_b(\mathrm{Fe}) = 6.0$ eV and $W_b(\mathrm{Pd}) = 5.86$ eV. Then the Fe-Fe hopping integrals are modified to take into account the different interatomic distances in bulk Fe and bulk Pd according to the d^{-5} law. Hopping integrals are neglected beyond the second nearest neighbors. The heteronuclear hopping integrals (Fe-Pd) are obtained as the geometric average of the corresponding homonuclear hopping integrals. This has been proved to be a very good approximation in calculations for embedded clusters,[28] bulk alloys,[29] and multilayers[30] of transition metals. Charge transfer effects are treated in the limit of large direct Coulomb repulsion $U(i)$ [i.e., $U(i) \to +\infty$ and $\Delta n(i) \to 0$ with $U(i)\Delta n(i)$ finite], which amounts to imposing local charge neutrality at each site i. This assumption can be justified in this case since, in the *ab initio* electronic structure calculations performed by Kuhnen and da Silva[12] of various Fe-Pd bulk alloys with different compositions, the electronic occupations were found to be independent of the Fe content in the alloys, as well as almost insensitive to small contractions and expansions around the equilibrium lattice parameter of the structures. The values for the intra-atomic exchange integrals J_{Fe} (0.67 eV), as well as for the d-band filling $n_d(\mathrm{Fe})$ (6.5) have been already used in previous works.[31] The determination of the corresponding parameters for Pd will be discussed in the next section.

III. STUDY OF AN ISOLATED Fe IMPURITY IN BULK Pd

In this calculation we must start from an accurate density of states for bulk Pd, i.e., the number of exact levels in the continued fraction giving the bulk Green function must be such that the density of states is converged. We have found that the densities of states (DOS) calculated with 25 and 30 levels are almost indistinguishable. Consequently, in the following all the local densities of states (LDOS) have been calculated with 30 exact levels (i.e., 60 exact moments). The DOS of bulk Pd, obtained with the hopping integrals determined as explained in Sec. II, is given in Fig. 1.

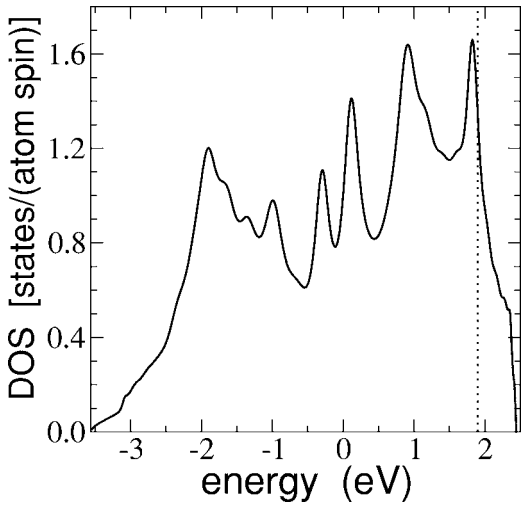

FIG. 1. The density of states (DOS) for fcc bulk Pd calculated within our tight binding scheme. The position of the Fermi energy, ε_F, is indicated by the dotted line.

The next step is to fix the value of the exchange integral J_{Pd} in Pd which is of prime importance in studying the magnetization induced by an Fe impurity on the neighboring Pd atoms. Bulk Pd is not magnetic at its equilibrium distance; J_{Pd} cannot be derived from the experimental magnetic moment as done for J_{Fe}. In the present model J_{Pd} is actually the Stoner parameter which can be calculated from the expression of the susceptibility, i.e., $\chi/\chi_0 = [1 - Jn(\epsilon_F)]^{-1}$ where $n(\epsilon_F)$ is the bulk density of states per atom and per spin at the Fermi level. Taking the value of χ/χ_0 and $n(\epsilon_F)$ from the *ab initio* calculations of Moruzzi *et al.*[27] yields $J_{\mathrm{Pd}} = 0.67$ eV.

We must now determine the number of d electrons per atom in Pd, $n_d(\mathrm{Pd})$. In *ab initio* calculations the Fermi level is located on the high-energy side of the peak close to the top of the d band at about 2/3 of its height. In our DOS this corresponds to a d-band filling lying in the range 9.2–9.3 electrons per atom. Note that in our calculation Pd would be magnetic in the bulk for a d-band filling belonging to the interval [8.85–9.15] and it would be physically unreasonable to have a d-band filling less than 8.85. An alternative way to determine $n_d(\mathrm{Pd})$ is to ensure that bulk Pd becomes magnetic when the lattice is expanded by 5% to 6% as found in *ab initio* calculations.[1–3] This leads to $n_d(\mathrm{Pd}) \simeq 9.25$ by taking into account that $n_d(\mathrm{Pd})$ increases by $\simeq 0.1$ electron[1] during this expansion. We have thus adopted this value. In our calculations we have neglected the perturbation due to the Fe atom beyond its N_sth nearest neighbors and the number N_s has been varied until the total moment induced by the Fe atom is stabilized. It has been found that this moment converges for N_s around 13–17. Indeed the comparison between the results obtained with $N_s = 13$ and $N_s = 17$ shows that the moments of the Pd atom beyond the 14th shell are less than $10^{-3}\mu_B$, so that the total spin magnetic moment is almost the same in both calculations ($2S_T \simeq 6.1\mu_B$). The variation of the

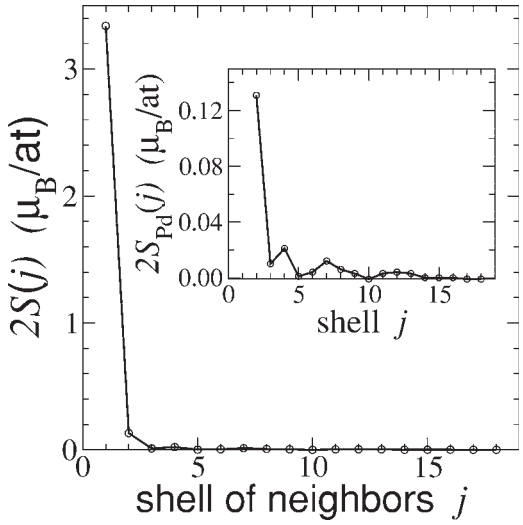

FIG. 2. Calculated local spin-magnetic-moment distribution $2S(j)$ for a single Fe impurity embedded in a bulk fcc Pd host. Here, $j=1$ defines the location of the Fe atom and $j=2-18$ specifies the different radial shells of Pd neighbors surrounding the Fe site. In the inset, we show similar results but where we plot, for the sake of clearness, only the local values at the Pd sites, $2S_{\mathrm{Pd}}(j)$.

local moment of a Pd atom as a function of the shell of neighbors of Fe is shown in Fig. 2. It is interesting to note that the moments of the Fe atom (almost saturated) and that of its nearest neighbors are almost independent of N_s and are in good agreement with previous *ab initio* calculations.[14] On the experimental side, Verbeek *et al.*[8] have found that the moment induced by an Fe atom in Pd varies rapidly with increasing Fe concentration. This can be inferred from our results since we predict that about 380 Pd atoms are polarized by a single Fe atom and thus, even at very low concentration, interference effects will occur between the polarization clouds associated with Fe atoms. The measurement at the lowest Fe concentration (0.27%) yields a moment of about $\simeq 7.3\mu_B$ per atom. Since we have found that about 380 Pd atoms are polarized (i.e., the radius of the polarization cloud is $\simeq 11$ Å) around a single Fe impurity we expect that below a concentration of 0.2–0.3 % the total moment per Fe atom should become rather constant so that our calculations are in good agreement with experiments.

Finally, it is interesting to look at the LDOS on the Fe atom and its first nearest neighbor Pd atoms (Fig. 3). The LDOS on the Fe atom [Fig. 3(a)] presents very qualitatively the same characteristics as those calculated on small clusters by Delley *et al.*[15] with a low density of occupied states and a high one above the Fermi level for spin down states. However, the details of the LDOS for both spins cannot be reproduced by the cluster calculations, the latter being strongly affected by the discrete character of the levels which is still very present in high symmetry clusters as small as 43 atoms, and by the large broadening (0.4 eV) of the discrete states chosen in Ref. 15. In particular the down-spin band on Fe [continuous line of Fig. 3(a)] exhibits a bound state above the d band of Pd (at $E=2.61$ eV) due to the t_{2g} orbitals of Fe and a quasibound state at $E=2.40$ eV close to the Pd band edge due to its e_g orbitals. Both are strongly localized on the

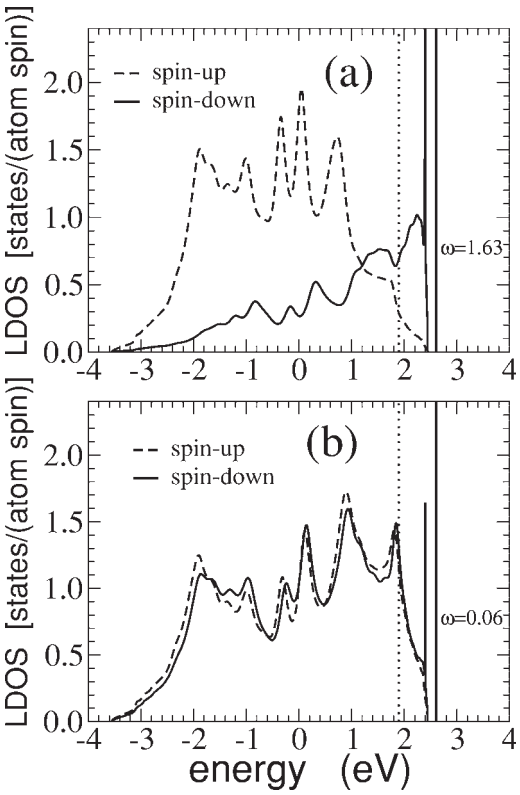

FIG. 3. The local density of states (LDOS) for (a) a single Fe impurity embedded in a bulk fcc Pd host and (b) at the first shell of nearest neighbors Pd atoms.The position of the Fermi energy, ε_F, is indicated by the dotted line. The vertical lines correspond to the t_{2g} bound state of spin down (see text) with a weight ω.

Fe atom. The LDOS of the Pd atoms belonging to the first shell of nearest neighbors of the Fe impurity shown in Fig. 3(b) are scarcely changed relative to that of bulk Pd, except from the small splitting between the up- and down-spin bands and the appearance of two small peaks at high energy in the down spin LDOS due to the tails of the two previously discussed localized states.

IV. STUDY OF FePd NANOPARTICLES

A. Geometry of the clusters

All considered clusters are a fragment of an fcc lattice and possess the cubic symmetry.[16,19,20] Atomic relaxation is neglected and, since we consider only a very small number of substitutional impurities in the Pd clusters, we have fixed the lattice parameter to the bulk equilibrium value for Pd. Indeed, taking relaxation into account would need huge computations for the sizes of clusters we are considering, and we do not expect that it would change the main trends, in particular, the chemical order in the cluster. As shown in Fig. 4, we consider two types of atomic arrangements in the clusters. The first type is closed-shell cuboctahedral clusters which, starting from a central atom, are built by adding its 12 NN atoms which gives the first shell. Then the second shell is obtained by adding the missing NN of the atoms of the first shell and the process is iterated until the desired number

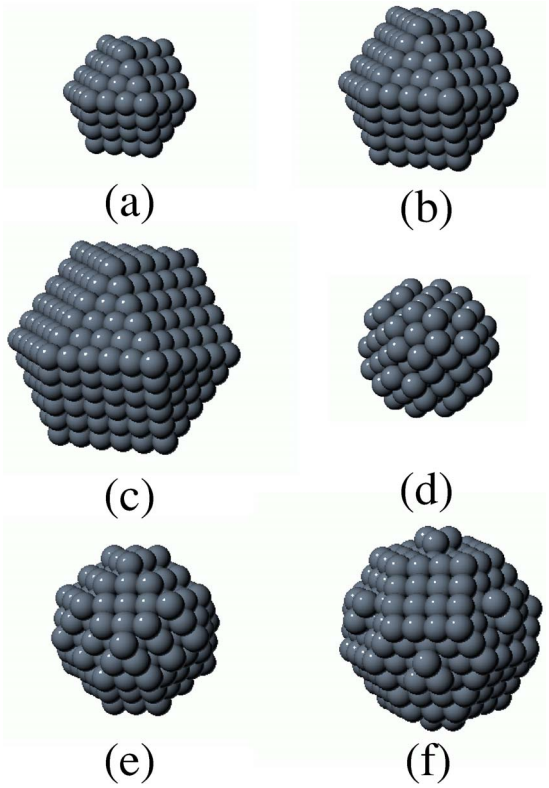

FIG. 4. Illustration of the geometrical structure of some representative Pd_N clusters considered in this work. In (a), (b), and (c) we show atomic configurations for cuboctahedral particles with $N=147$, 309, and 561, respectively, while in (d), (e), and (f) we show the structure of spherical clusters with $N=135$, 249, and 429, respectively.

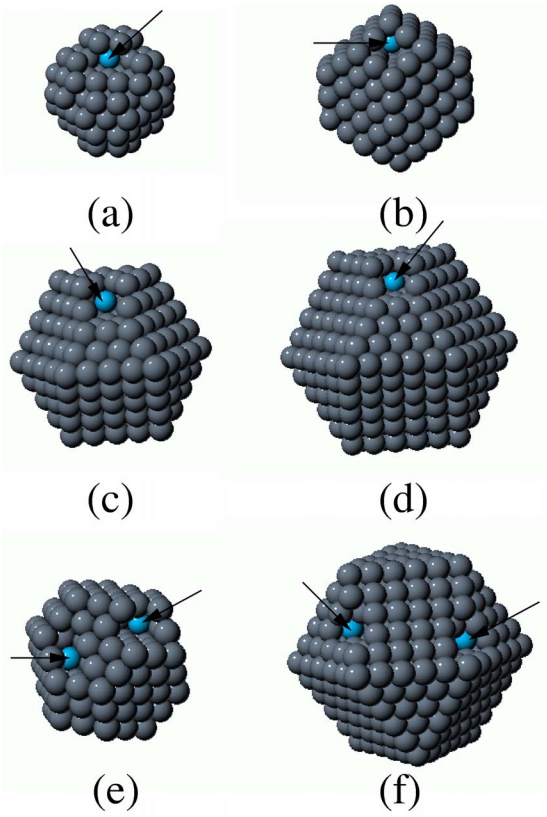

FIG. 5. (Color online) Illustration of some representative lowest energy atomic configurations for one and two Fe impurities embedded in Pd_N nanoparticles. In (a) and (b) we show the lowest energy array for spherical $Fe^{eq}Pd_{134}$ and $Fe^{eq}Pd_{200}$ clusters, respectively. (c) and (d) illustrate the equilibrium configurations for cuboctahedral $Fe^{eq}Pd_{308}$ and $Fe^{eq}Pd_{560}$ nanoparticles, respectively, and finally, (e) and (f) show the lowest energy structure for spherical $Fe_2^{eq}Pd_{199}$ and cuboctahedral $Fe_2^{eq}Pd_{559}$ clusters, respectively. In all the figures, some Pd atoms have been removed from the surface to put more clearly in evidence the position of the Fe impurities (marked with arrows).

of shells is attained [see Figs. 4(a)–4(c) for 147-, 309-, and 561-atom structures, i.e., 3, 4, and 5 shells, respectively]. These clusters are homothetic and present eight (111)-like triangular and six (100)-like square facets. The second type of clusters are spherical. They are built from a central atom by adding its successive shells of neighbors until a given radius [see Figs. 4(d)–4(f) for 135-, 249-, and 429-atom clusters, respectively]. For more than two shells of neighbors, this type of construction leads to the formation of cluster structures with sizes, shapes, and surface terminations different from the closed-shell ones. As will be seen in the following, this will strongly influence the spatial distribution of Fe impurities in the particles, as well as the magnetic properties of the Fe-Pd cluster alloys.

B. Optimal positions of the Fe impurities

The optimal positions of a single Fe atom within our considered Pd nanoparticles is obtained by calculating the total energy of the $Pd_{N-1}Fe$ clusters in which the Fe impurity occupies successively each geometrically inequivalent site. In Fig. 5 we show some representative examples of our calculated lowest-energy atomic configurations in which several Pd atoms of the surface have been removed in order to more clearly evidence the internal position of the Fe impurities (indicated by arrows). Note that, in most cases, in particular when the cluster is large enough, the Fe atom is located at the site the farthest from the center, having, however, its complete shells of nearest and next nearest neighbors (NNN). Thus, the Fe atom is directly bound to Pd atoms belonging to the outermost atomic shells of the particle (see Fig. 5). Indeed, it is energetically favorable to have the maximum number of NN and NNN Fe-Pd bonds in the cluster. This can be easily seen by comparing the contributions of Pd-Pd and Fe-Pd pairs in the sum of exponentials appearing in the attractive and repulsive terms of the potential [Eq. (1)]. It is found that both for NN and NNN bond lengths the contribution of a Fe-Pd bond is larger than that of a Pd-Pd bond in the attractive term, while the NN repulsive interaction is decreased when replacing a Fe-Pd pair by a Pd-Pd one, the NNN pair interaction being almost unchanged. Thus, the Fe atoms should be inside the cluster and not at the surface. Let us now consider the Pd atoms which are directly bound to the Fe atom. The contribution to the total energy of these Pd atoms is obviously lowered by the presence of one Pd-Fe bond. However, the smaller the coordination of the Pd

atom, the larger this lowering of energy. This is due to the many-body nature of this potential since $\alpha<1$. Consequently, the total energy of $Pd_{N-1}Fe$ clusters reaches its minimum when the Fe atom belongs to the subsurface region so that some of their Pd neighbors have incomplete NN and NNN shells. In fact, this environment dependence is at the origin of the strong variations for the position of the single Fe impurity observed in Figs. 5(a)–5(c), since if we change the surface termination of the particles (by increasing the size of the Pd host) the Fe atom is forced to change its position (occupying subsurface regions below edges, corners, triangular and square facets) in order to have the most favorable Pd environment. As a consequence, in clusters with n closed shells, the Fe atom will always occupy the same type of sites, namely in the $(n-1)$th shell when the size is large enough and in the vicinity of the corners [see Figs. 5(c) and 5(d)], whereas in spherical clusters the atomic environments of the Pd atoms bound to the Fe atom may be very different.

The optimal positions of two Fe atoms have been deduced from the calculation of the total energy for all possible configurations. The results show that when the cluster size is large enough, the two Fe sites can be determined by maximizing the number of Fe-Pd NN and NNN bonds and, in addition, they must be sufficiently far from each other so that they do not share a NN or NNN Pd atom [see Figs. 5(e) and 5(f)]. Let us first explain the former condition. The tendency to form NN (NNN) Fe-Pd bonds is governed by the difference in energy between the sum of contributions of Pd-Pd and Fe-Fe pairs minus twice the contribution of a Fe-Pd pair. This quantity is almost vanishing for the repulsive interactions while the formation of a NN (NNN) Fe-Fe pair is energetically unfavorable in the attractive term. This first condition does not prevent the two Fe atoms to share NN or NNN Pd atoms. However, due to the attractive part of the potential, two Pd atoms, each of them bound to one Fe atom, are energetically more favorable than one Pd atom bound to the two Fe atoms so that, finally, in the best configuration the two Fe atoms should not share NN and NNN Pd atoms. This can be always be realized when the size of the cluster is large enough. Note that, in the latter case, several geometrically inequivalent configurations may have the same energy.

Using the same arguments as above, we predict that the lowest energy configuration for Fe atoms in the vicinity of a Pd semi-infinite crystal will be neither in the surface layer nor in the bulk, but rather in the subsurface region. This is in qualitative agreement with experimental and theoretical studies addressing the surface alloying in ultrathin Fe films deposited on Pd(001),[10] where it has been found that the composition profile is consistent with a sublayer Fe film located under one monolayer (ML) thick Pd capping layer. In fact, such sublayer confinement of a film element with a surface free energy larger than that of the host element has been also reported in Fe/Au(001),[32] Pd/Cu(100),[33] Ni/Ag(001),[34] and Mn/Ag(001)[35] films. In general, the existence of subsurface species has been found to strongly influence the roughness of the surface, the local moment distribution, as well as the low energy orientation of the magnetization in the system. In addition, in a recent work, Kitchin *et al.*[36] have demonstrated that in the case of Pt(111) films, the existence of 3*d* transition metal sublayers (e.g., Ti, V, Cr, Mn, Fe, Co, and Ni) strongly affects the chemical and electronic properties of the material, resulting in weaker dissociative adsorption energies of hydrogen and oxygen on these surfaces, a result that could have important implications in the context of catalyst design.

In the case of bimetallic nanoparticles the stability of well-defined single-component subsurface layers has been recently theoretically predicted by Baletto *et al.*[37] These authors have found, by performing classical molecular dynamics simulations, that in the cases of Ag/Pd, Ag/Cu, and Ag/Ni core-shell nanoparticles, depending on the temperature and on the morphology of the preformed Ag core, the deposited Pd, Cu, and Ni atoms present a strong tendency to accumulate in the layer just below the surface, thus forming a well-defined intermediate layer. Interestingly, for all the elements forming stable sublayers it was found that, when they exist as single isolated impurities in the Ag host, the most favorable position is located, as in our case, below the cluster surface below edges and vertices. We believe that our results are particularly interesting since our magnetic Fe subsurface species might induce a strong polarization at the neighboring surface Pd sites that could lead to a wide variety of magnetic behaviors since now, in contrast to the bulk environment, the magnetic response of our finite host is expected to be strongly influenced by the size and the surface termination of the nanoparticles. In addition, it is clear that the electronic structure of the external Pd atomic shells will be considerably perturbed by the presence of the subsurface species, strongly changing their electronic and catalytic behavior. As a consequence, the magnetic and electronic properties of our Fe-dilute Fe-Pd cluster alloys will be extensively analyzed in the following.

C. Magnetic behavior of Fe-dilute Fe-Pd nanoparticles

In this section we present electronic structure calculations in order to analyze the magnetic behavior of the previously obtained lowest energy chemical order in our Fe-Pd cluster alloys. We will focus on the dependence of the magnetic properties on relevant variables such as Fe-impurity content, surface structure, and particle size. Finally, we will show how, by combining the theoretical calculations of the orbital-to-spin ratio with x-ray magnetic circular dichroism experiments, very precise features of the chemical order in this kind of magnetic nanostructures could be obtained.

In Fig. 6 we show first the evolution of the calculated local spin moment distribution $2S(j)$ at each shell of neighbors j for unrelaxed open-shell $FePd_{134}$, $FePd_{248}$, and $FePd_{428}$ clusters [see Figs. 4(d)–4(f) for representative examples], as well as for closed-shell $FePd_{146}$, $FePd_{308}$, and $FePd_{560}$ particles [such as the ones shown in Figs. 4(a)–4(c)] with nearest neighbor distances equal to the bulk Pd one. We consider a fixed number of electrons per site $n_d(\mathrm{Fe})=6.5$ and $n_d(\mathrm{Pd})=9.25$ as previously discussed in Sec. II B and Sec. III. Note that both values are of the order of the number of *d* holes used in various magnetic circular x-ray dichroism experiments performed on ultrathin Fe/Pd(100) films,[38] Pd/Fe multilayers,[39], and Fe-Pd macroscopic alloys.[40] In all clusters, the Fe atom is placed at the center of the particles in

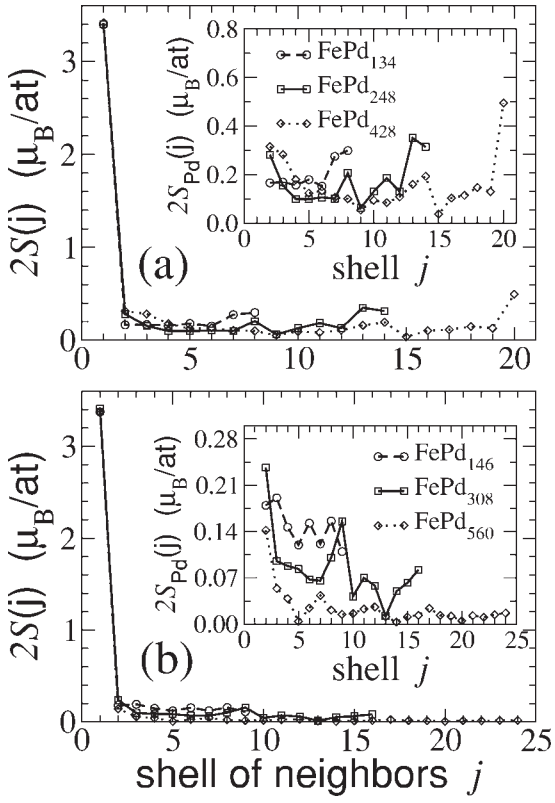

FIG. 6. Calculated local spin magnetic-moment $2S(j)$ at each shell of neighbors j for representative single Fe-doped nanoparticles. In all cases, the Fe impurity is always placed at the center ($j=1$) of (a) spherical and (b) cuboctahedral clusters of different sizes. In the insets we plot, for the sake of clearness, only the local values at the Pd shells, $2S_{\mathrm{Pd}}(j)$.

order to try to simulate the local atomic environment of the Fe-dilute Fe-Pd macroscopic alloys. It is clear that the inclusion of the Fe impurity affects the local magnetic moments at the neighboring Pd sites (see also the inset of both figures) leading to the formation of the expected polarization cloud having a spatial form that strongly depends on the local atomic environment. In particular, the values for the local spin magnetization at the nearest Pd atoms surrounding the Fe impurity, $2S(2)$, present strong oscillations when increasing the size of the Pd host and actually, in our biggest considered cluster (having the most bulklike atomic environment), Pd_{561}, the induced maximum Pd moment is at the nearest Pd sites and equal to $0.14\mu_B$/atom [see the inset of Fig. 6(b)], a value that is in good agreement with the DFT calculations of Oswald *et al.*[14] performed on Fe-dilute Fe-Pd alloys and with our results for a single Fe impurity embedded in a bulk fcc Pd host shown in Fig. 2. Actually, by looking at the magnetization profiles shown in the insets of Fig. 2 and Fig. 6(b) for the $FePd_{560}$ nanoparticle, we see that both infinite and finite systems have very similar local moment distribution in which a decreasing oscillatory behavior is obtained with well-defined maxima at $j=7$ and 12. In the bulk structure, almost zero values for $2S(j)$ are found for $j \geqslant 15$ while, at the cluster system, spin moments of the order of $0.02\mu_B$/atom are still obtained due to the strong surface contributions.

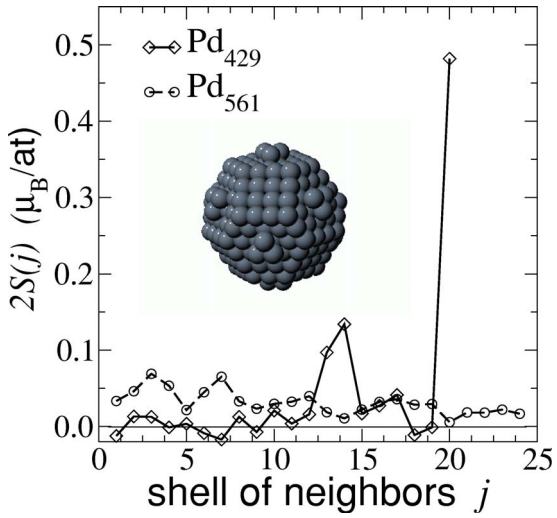

FIG. 7. Calculated local spin magnetic-moment $2S(j)$ at each shell of neighbors j for spherical Pd_{429} and cuboctahedral Pd_{561} clusters. In the inset, we show the surface structure of the Pd_{429} particle; note that the 20th shell corresponds to the three atom islands at the center of the (111) facets.

From both Figs. 6(a) and 6(b) we observe that, when moving out from the center of the particles, the local moments oscillate; however, we note that at the most external Pd sites, the values of $2S(j)$ are strongly affected by the surface termination of the particles. In particular, we note from Fig. 6(a) that when the surface is composed of small ad-islands located at the facets of the particles [see Figs. 4(d), 4(e), and 4(d)], the surface considerably increases its average magnetization, leading (as we will see in Fig. 7) to appreciable changes in the total spin magnetization $2S_T$ in the particles. Interestingly, from Fig. 6(b) we note that for $FePd_{560}$ which presents the most extended perfectly flat facets [see Fig. 4(c)] almost magnetically dead surface layers are found. For the sake of comparison we have carried out calculations using our spin-polarized self-consistent tight-binding approach for (111) and (100) semi-infinite crystals in which the LDOS were derived from a continued fraction with 30 exact levels. We have found that these surfaces are not magnetic, a fact that is consistent with the results on $FePd_{560}$.

It is important to comment that the trend of a magnetic enhancement observed at the surface Pd sites in Fig. 6(a) is also obtained, although less pronounced, in pure Pd nanoparticles as shown in Fig. 7. It is thus interesting to compare our magnetization data shown in the figure for pure spherical Pd_{429} and cuboctahedral Pd_{561} clusters with the recent experimental works of Sampedro *et al.*[41] and of Shinohara and co-workers[42] where the existence of a well-defined average magnetization in nanometer-sized Pd particles has been established. Both groups have proposed different explanations for their measurements. On the one hand, Sampedro *et al.* argue that the measured magnetization is due to the presence of internal defects in the clusters while, on the other hand, Shinohara and co-workers claimed that it is instead the reduced local coordination of the Pd atoms forming the (100) facets that is at the origin of the magnetic behavior observed

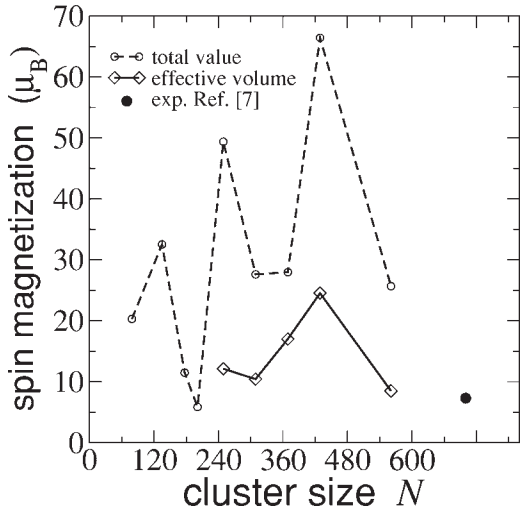

FIG. 8. Calculated total spin magnetization (dashed line) for the single Fe-doped Pd nanoparticles in which the Fe atom is at the center. The continuous line shows, for some representative examples, the spin magnetization of an effective volume of the particles (as defined in the text).

in their samples. From our calculations on Pd(100) and Pd(111) surfaces, as well as for the pure Pd_{561} particle, we expect that, when increasing the size of the particles, cluster surfaces containing perfectly flat (111) and (100) facets will not be magnetic. However, following our theoretical data for the pure Pd_{429}, we can speculate that the existence of Pd nanoparticles having low coordinated atoms adsorbed in the last shell, that is, a rather open or corrugated cluster surface could contribute to the measured data, although a role played by inner defects cannot be excluded.

In Fig. 8, we show now the calculated total spin magnetization of single Fe-doped Pd nanoparticles, in which the Fe atom is at the center as a function of the cluster size N. Following the complex local moment distribution shown in Fig. 6, we can see that the total moment exhibits complex oscillatory variations. In particular, the high values found for $N=249$ and 429 originate, as already discussed in the previous paragraphs, from strong surface contributions, while the very low values obtained for $N=177$ and 201 are due to the existence, in the former, of antiferromagnetic configurations (not shown) between the local moment at the Fe site and some of the Pd atoms in the structure and, in the latter, to a less effective polarization of the Pd host. It is thus clear that the presence of peaks and valleys in the LDOS around the Fermi level is very sensitive to the local atomic environment and could be at the origin of the sizable quenchings, enhancements, or changes of sign in the local moments observed in the structures.

Actually, in order to roughly eliminate the surface contributions and to analyze more clearly the convergence of the induced polarization to the bulk value as a function of N, it is convenient to define an effective (reduced) volume in the particles in which only the local contributions to the total magnetization of the Pd atoms, having their complete first and second shells of neighbors, is taken into account. The total magnetization of this effective volume for $N=249$, 309, 369, 429, and 561 plotted also in Fig. 8 shows, as expected, less pronounced variations as a function of cluster size and actually, we note that for the largest considered 561-atom structure, the total magnetization of this effective volume is already very close to the total induced moment ($6.1\mu_B$) that we have found for an isolated Fe impurity in bulk Pd (see Sec. III) and to the experimental measurements performed on Fe-dilute Fe-Pd alloys[8] that estimate the formation of giant moments around the impurities of the order of $7.3\mu_B$ (see the isolated point in the figure).

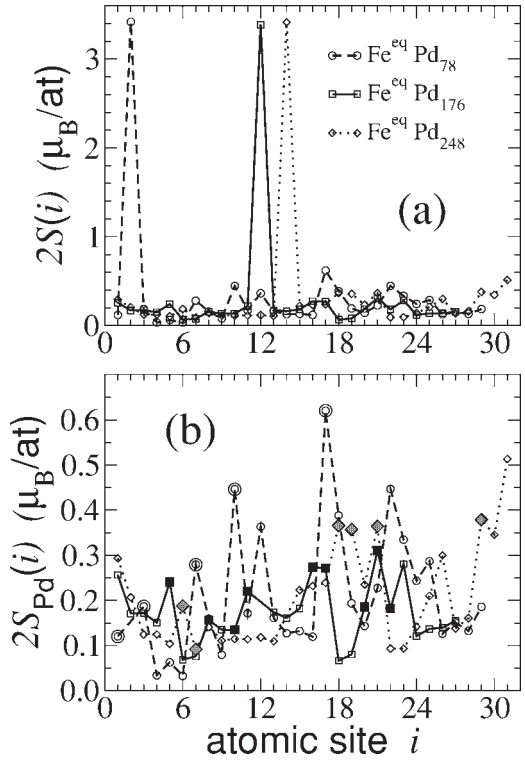

FIG. 9. (a) Calculated local spin magnetic moments $2S(i)$ at each site i for the lowest energy location of a single Fe impurity embedded in various Pd nanoparticles. As in previous cases, we show in (b) the local spin moments only at the Pd sites for the same structures. The sites marked with double circles, filled squares, and gray rhombuses define the locations of the nearest-neighbor Pd atoms surrounding the Fe impurity.

However, as clearly stated in the previous section, Fe-dilute Fe-Pd nanoparticles are characterized by a well-defined chemical order in which the Fe atoms are located just below the surface of the particles. It is clear that the low symmetry position of the iron impurities, the finite size of the host, and the localization effects present at the cluster surface will strongly change the local moment distribution in the Pd host (with respect to the one presented in Fig. 6) and thus modify the average magnetization of the particles.

In Fig. 9 we show the local moment distribution at each site i, $2S(i)$, for single Fe-doped Pd particles but where the iron impurity is located in their optimal position (Fe^{eq}). In these cases, the low symmetry location of the Fe species, together with the relatively large number of atoms forming the nanoparticles is expected to lead to the existence of cluster structures with a high number of inequivalent sites and, as

a consequence, the study of large Fe-dilute Fe-Pd nanoparticles requires a large amount of computer time. However, in our considered Fe-dilute Fe-Pd cluster alloys, even if the local magnetization at all the Pd sites is perturbed by the inclusion of the Fe atoms, we have observed that several Pd atoms belonging to a well-defined radial shell, but located far away from the iron impurities, have values of $2S(i)$ which are almost the same as those obtained in the corresponding pure Pd_N clusters (variations of 10^{-2} and $10^{-3}\mu_B$ are obtained). As a consequence and for the sake of simplicity, we will consider them as being geometrically equivalent in order to slightly reduce the computer time in our calculations. Still, as we will see in the following, cluster structures with sizes of ~250 atoms and having as large as 35 inequivalent sites need to be solved. Therefore, we have chosen some simple, computationally tractable, examples and then try to infer from these results the implications for more concentrated Fe-Pd alloys. In Fig. 9(a) we show the values of $2S(i)$ for $Fe^{eq}Pd_{78}$, $Fe^{eq}Pd_{176}$, and $Fe^{eq}Pd_{248}$ cluster alloys and, in Fig. 9(b), we plot as in previous cases (for the sake of clarity) the local moment distribution only at the Pd sites for the same systems and where we have marked with double circles, filled squares, and gray rhombuses the nearest neighbor Pd atoms surrounding the Fe impurity for each one of the considered clusters. It is clearly seen [Fig. 9(a)] that the spin moment of the iron impurity is almost insensitive to the different locations within the structures (being always quasisaturated, i.e., $\sim 3.4\mu_B$). However, as we will see in the following, this will not be the case for the orbital moment which has been found to be highly sensitive to the precise details of the local atomic environment, a sensitivity that could be used to identify relevant features of the chemical order in the particles.

From Fig. 9 we note that, in contrast to the Fe atom, the magnetic response of the Pd atoms is strongly affected by the off-center position of the iron impurity. This is clearly seen, for example, in the case of the $FePd_{248}$ alloy [compare the inset of Fig. 6(a) with the results shown in Fig. 9(b)] where in the equilibrium configuration it is more common to find local contributions of the order (greater) of (than) $0.2\mu_B$. Interestingly, and following the trend observed in Fig. 6(a), we have found that the Pd sites that are first nearest neighbors of the Fe impurity do not always carry the largest local spin moment. In fact, the largest enhancement observed in the 249-atom structure is obtained for the surface site $i=31$, which is located at a distance of 16 Å from the Fe impurity. In contrast, for the smallest 79-atom cluster, the largest value of $2S(i)$ is obtained for a surface atom located just above the iron impurity (see the results for $i=17$), a result that illustrates the complex interplay between surface and hybridization effects in determining the general magnetic behavior of the particles.

Actually, from Fig. 10 in which we plot the total spin magnetization for our two types of chemical order we note that, at least for the smallest sizes, different locations of a single iron impurity can considerably affect the total magnetization of Pd clusters. It is thus clear that an accurate characterization of the chemical order in bimetallic Fe-Pd nanoparticles is a prerequisite for a deeper understanding and modeling of their properties.

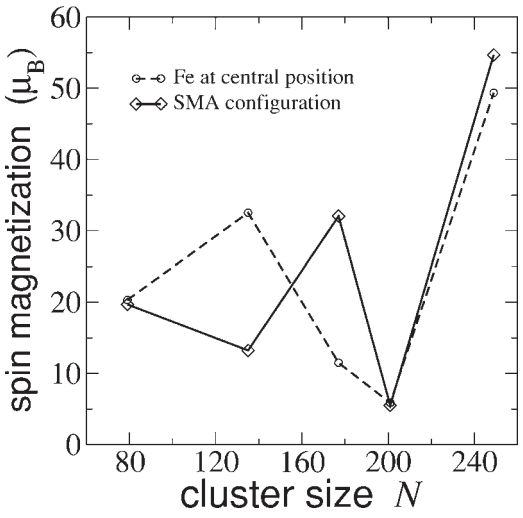

FIG. 10. Calculated total spin magnetization for single Fe-doped Pd clusters.

Of course, we note that for the more concentrated alloys, there will be an additional factor that complicates the interpretation of the magnetization data in these kinds of nanoalloys, and that is related to the possibility of having several Fe atoms not very far from each other. These types of atomic arrays will perturb further the magnetic response of the Pd host due to the expected strong interference effects between the various Fe-induced polarization clouds. In principle, in the dilute limit with increasing the Fe content, we exchange weakly magnetic Pd atoms by Fe species with high spin states and, as a consequence, the total magnetization in the system must increase. This is actually what we observe from Fig. 11 where we plot the local moments $2S_{Pd}(i)$ for each type of Pd site i in the 249-atom cluster having up to three Fe atoms located at their lowest energy positions. The number of geometrically inequivalent Pd atoms increases rapidly with the number of impurities and we have represented by a single point all atoms having very close spin moments. The values of $2S_{Fe}(i)$ have been excluded from the figure since, as in previous cases, the spin moment of the Fe impurities was found to be almost insensitive to their different locations within the structure, being always quasisaturated and of the order of $3.4\mu_B$. From Fig. 11 we note that the inclusion of the Fe impurities considerably enhances the local magnetization in all the regions of the structure and actually, we have found that the total magnetization increases from 9.3, 54.7, 65.6, and $71.5\mu_B$ when going from the Pd_{249} to the $Fe^{eq}Pd_{248}$, $Fe_2^{eq}Pd_{247}$, $Fe_3^{eq}Pd_{246}$ cluster alloys, respectively. In the latter two structures, the different distances between the Fe atoms are of 8.7 and 11 Å and, even if the magnetic impurities are well separated from each other, the nonlinear behavior obtained for the total magnetization as a function of the Fe content indicates that the neighboring polarization clouds (with a diameter of ≃22 Å in the bulk) are still interacting with each other. Actually, as we will see in the following, there are some cases in which the interference between the Fe-induced polarizations can lead also to appreciable reductions of the total magnetization in Fe-Pd nanoparticles.

The results discussed in the previous paragraphs could be important in real systems since variations in composition in

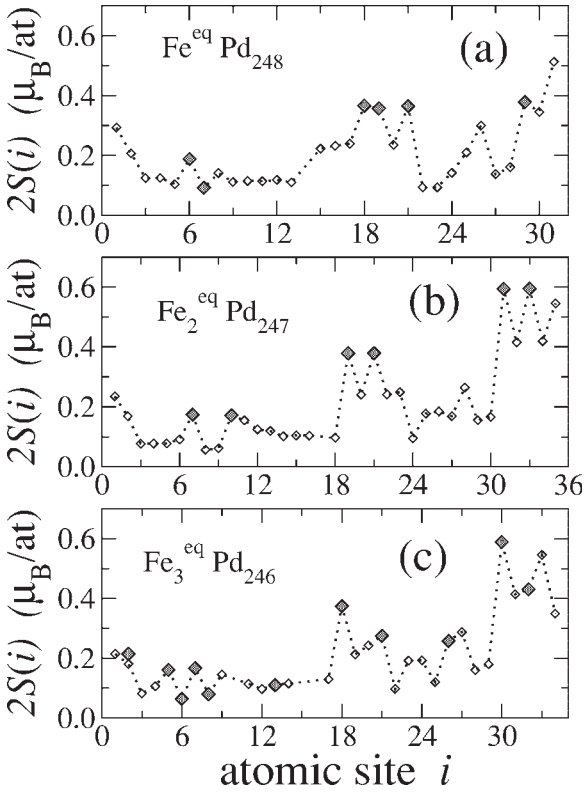

FIG. 11. Calculated local spin magnetic moments $2S_{\mathrm{Pd}}(i)$ at each site i for (a) one, (b) two, and (c) three Fe impurities substituted, at their lowest energy position, in a 249-atom Pd host. The sites marked with gray rhombuses define the locations of the nearest neighbor Pd atoms surrounding the Fe impurities.

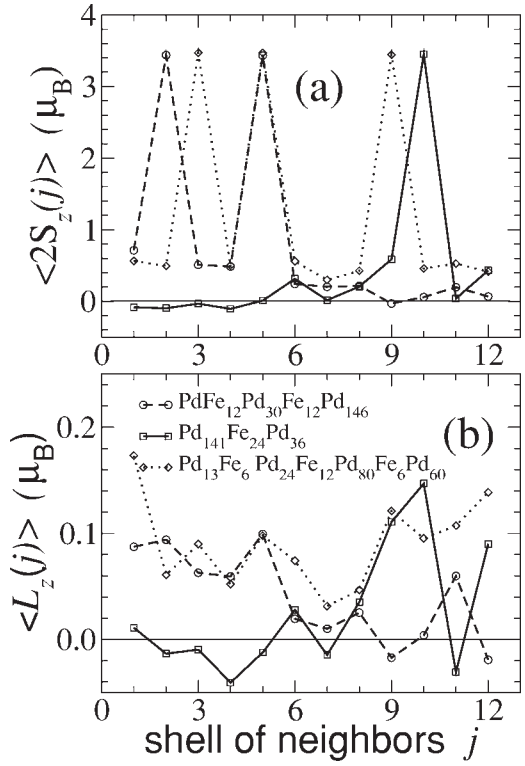

FIG. 12. Calculated average (a) spin $\langle 2S(j)\rangle$ and (b) orbital $\langle L_z(j)\rangle$ magnetic moments at each shell of neighbors j for the $Fe_{24}Pd_{177}$ bimetallic cluster having different degrees of alloying (as defined in the text).

well-defined volumes of Fe-Pd cluster alloys, or the existence of homogeneous distribution of both Fe and Pd species, can result in a large range of magnetization values, depending on the size and shape of the surface. As is well known, the atomic organization of the different species inside bimetallic nanoparticles depends on the fabrication technique, as well as on the experimental parameters controlling the synthesis procedure (e.g., temperature, solvents, etc.). In general these synthesized Fe-Pd particles exhibit chemically disordered configurations. However, the annealing of the samples can induce the constituent atoms to rearrange themselves and, around specific concentrations, this rearrangement can give rise to long-range ordered cluster alloys. As a consequence, it could be possible to tune the properties of this type of nanoclusters, not only by varying their size and composition, but also their chemical order. This fact has been already clearly demonstrated in the case of Fe-Pd thin films by Bernas *et al.*[43] who, by means of He ion irradiation, have found that the transformation from chemical disorder to order could be accurately controlled.

In order to qualitatively analyze the previous effects, we consider the case of a 201-atom Pd cluster but in which we introduce, as substitutional impurities, a total of 24 Fe atoms in different high symmetry locations, i.e., distributed in radially layered structures. We do not attempt to obtain the lowest energy chemical order and consider here three types of atomic configurations in which the Fe atoms are first mainly located in the core region and at two different radial distances from the center of the particles forming the $PdFe_{12}Pd_{30}Fe_{12}Pd_{146}$ alloy, then a second segregatedlike configuration in which the iron impurities are at surface sites defining the $Pd_{141}Fe_{24}Pd_{36}$ structure and, finally, a radially multilayered structure forming the $Pd_{13}Fe_6Pd_{24}Fe_{12}Pd_{80}Fe_6Pd_{60}$ compound. In Fig. 12(a), we show the values for the average spin moment $\langle 2S(j)\rangle$ at each shell j [$j=1$ (central atom), 2–12] for these types of chemical order. It is seen that, as in previous cases (i) the average spin moment at the radial shells formed by Fe atoms is almost insensitive to their position within the Pd host having values in the range of $3.43-3.47\mu_B$ and that (ii) the spin magnetic moment $\langle 2S(j)\rangle$ at the radial layers exclusively formed by Pd species is strongly affected by the internal distribution of the Fe impurities. In particular, note that for the atomic configuration in which the Fe atoms are occupying surface sites in the particle, a less effective polarization of the Pd host is found (see the continuous line), together with the existence of an antiferromagnetic configuration between the pure Pd core region and the outermost Fe-Pd alloyed external shells. The average magnetic moment of this atomic array is equal to $0.55\mu_B$/atom. In addition, when the Fe atoms are mainly located at the inner sites (dashed line), a ferromagnetic configuration is now obtained together with a notable enhancement (decrease) of the spin moments in the Pd sites of the core (surface) region, a result that produces only a slight increase in the average spin magnetization now equal to $0.6\mu_B$/atom. Interestingly, in the more alloyed (radially lay-

ered) $Pd_{13}Fe_6Pd_{24}Fe_{12}Pd_{80}Fe_6Pd_{60}$ array, a more effective induced polarization is found in all the Pd sites of the structure, increasing the average spin magnetization to $0.82\mu_B$/atom.

From our results shown in Fig. 12(a), it appears that the strong sensitivity of the magnetic response of the Pd atoms to the precise location of the iron impurities within the structures can lead to a wide variety of macroscopic behaviors. Even if we have found that low-energy configurations are obtained when the Fe atoms are located in the subsurface region of Pd nanoparticles, some experimental techniques involving high temperatures and rapid cooling of the samples can lead to the formation of Fe-Pd nanoalloys characterized by metastable chemical configurations, and, as a consequence, the precise knowledge of the spatial distribution of the magnetic impurities is of fundamental importance for a correct interpretation of the measured data.

At this point, we must stress that precise information concerning the way that different species are organized inside a particle is a very complex issue and requires the use of element sensitive techniques. In this respect, gas adsorption[44] and x-ray magnetic circular dichroism (XMCD) experiments[45] have been revealed to be powerful tools in order to obtain an acceptable chemical characterization in composite materials. In particular in the latter, the application of the sum rules in the analysis of the XMCD measurements links the measured spectra to the value of the spin $2S$ and orbital L magnetic moments per atom and actually, the study of their ratio, $L/2S$, as a function of composition and structural parameters of the samples give valuable information concerning precise microstructural features. In fact, due to the element selectivity of XMCD, only the properties of well-defined chemical species can be explored. This has been clearly established in the reports of Kamp *et al.*,[40] Le Cann and co-workers,[38] and of Vogel *et al.*,[39] who have analyzed several Fe-Pd thin films and have found strong variations in the spin and orbital magnetic moments due to changes in the chemical order. In the case of nanoparticles systems, Ulmeanu *et al.*[46] have determined the orbital-to-spin ratio in Fe-Pt clusters for different Fe contents and have obtained a stronger concentration dependence than the one found for Fe-Pt bulk samples.

From the point of view of theory, the calculation of the orbital magnetic moment requires the inclusion of the spin-orbit (SO) interaction H_{SO} in the Hamiltonian. This has been already done in previous works.[31,47] Briefly, the additional SO coupling term is written as

$$H_{\mathrm{SO}} = \sum_{i,\lambda\sigma,\mu\sigma'} \xi_i (\vec{L}_i \cdot \vec{S}_i)_{\lambda\sigma,\mu\sigma'} c^+_{i\lambda\sigma} c_{i\mu\sigma'}, \tag{6}$$

in the usual intra-atomic single-site approximation. Here, ξ_i stands for the SO coupling constant at atom i (i.e., ξ_{Fe} and ξ_{Pd}) and $(\vec{L}_i \cdot \vec{S}_i)_{\lambda\sigma,\mu\sigma'}$ refer to the intra-atomic matrix elements of $\vec{L}\cdot\vec{S}$ which couple the up- and down-spin manifolds and which depend on the relative orientation between the magnetization direction δ and the cluster lattice. Due to the inclusion of the SO interaction, the rotational invariance of the electronic Hamiltonian is no longer preserved and H depends now on the orientation of the magnetization in the system. Consequently, the total energy, the local densities of states, the spin magnetic moments, and the orbital magnetization all depend on δ and are defined as E^{δ}, $\rho^{\delta}_{i\lambda\sigma}(\varepsilon)$, $2S_{\delta}$, and L_{δ}, respectively. Finally, the component of the local orbital moment $L_{\delta}(i)$ on direction δ at each cluster site i is obtained from

$$L_{\delta}(i) = \sum_{\sigma} \sum_{m=-2}^{m=2} \int_{-\infty}^{\varepsilon_F} m\rho^{\delta}_{im\sigma}(\varepsilon) d\varepsilon, \tag{7}$$

where the real d orbitals have been transformed into the complex spherical harmonics basis and m refers to the magnetic quantum number. Here, the quantization axis of the orbital momentum is the same as the spin quantization axis.

As representative examples, we have decided to calculate the local orbital contributions for the previously discussed radially layered structures for which the spin-magnetic moments have been presented in Fig. 12(a). Our aim is to look for the existence of well-defined features in the values of L^{Fe}_{δ} and in the ratio $L^{\mathrm{Fe}}_{\delta}/2S^{\mathrm{Fe}}_{\delta}$, characterizing the different chemical configurations. In all cases, we choose the direction $\delta = z$, which is along a principal symmetry axis C_4 of the cluster. The presence of a magnetization in a given direction breaks the cubic symmetry so that the atoms belonging to the same coordination shell are no longer equivalent, resulting in a complex distribution of inequivalent sites that varies when the orientation of the magnetization is changed. Consequently, and for the sake of clarity, only the values for the average orbital moment $\langle L_z(j)\rangle$ at each shell of neighbors j are shown in Fig. 12(b). We note, in agreement with the behavior previously observed for the local spin moments on Pd atoms (see Figs. 6, 9, and 11), that remarkable variations at both inner and surface sites are also found for $\langle L_z(j)\rangle$. However, contrary to the $\langle 2S(j)\rangle$ distribution where the Fe species always have the highest spin states, in Fig. 12(b) we note that some Pd sites can have larger values of $\langle L_z(j)\rangle$ than the Fe impurities (see the results for the $Pd_{13}Fe_6Pd_{24}Fe_{12}Pd_{80}Fe_6Pd_{60}$ compound) due to their larger spin-orbit coupling constant ξ (i.e., $\xi_{\mathrm{Fe}}=0.05$ eV while $\xi_{\mathrm{Pd}}=0.19$ eV). Most importantly, the value of the orbital moment at the iron sites $\langle L^{\mathrm{Fe}}_z\rangle$ is notably affected by their precise location within the structures. Interestingly, when the Fe impurities are located in the core region of the Pd particle, they always have a well-defined orbital moment that slightly varies in the range of $0.09-0.10\mu_B$ (see results for $j=2$, 3, and 5), a value comparable to that of bulk Fe, where XMCD measurements give an orbital moment of $0.09\mu_B$.[48] Similar (almost constant) values have been found also in Fe-Pt alloys where for the $FePt_3$, FePt, and Fe_3Pt compounds L^{Fe} goes from 0.1, 0.11, and $0.09\mu_B$, respectively.[46] However, when Fe atoms are located at surface sites, enhanced orbital moments, of the order of 0.12 and $0.14\mu_B$ (see the results for $j=9$ and $j=10$ for the $Pd_{13}Fe_6Pd_{24}Fe_{12}Pd_{80}Fe_6Pd_{60}$ and $Pd_{141}Fe_{24}Pd_{36}$ cluster alloys, respectively) are obtained. This result clearly illustrates the strong localization effects present at the cluster surface.

It is also interesting to calculate the (easily) experimentally accessible orbital-to-spin ratio for the chemical configu-

rations investigated in Fig. 12. From our theoretical data we have found, as a consistent trend, that in all the cluster alloys the Fe atoms located as bulklike impurities have a well-defined $L_z^{\mathrm{Fe}}/2S_z^{\mathrm{Fe}}$ ratio ranging from 0.025–0.028. On the contrary, for surfacelike positions, Fe species have an enhanced ratio of the order of 0.035 (see the results for the dotted line with $j=9$) and 0.042 (see the continuous line for $j=10$), due to the increase of the orbital magnetic moment since the spin values stay almost constant. Thus, this quantity could provide valuable information in order to try to identify the existence of iron surface segregation or the formation of core-shell structures in Fe-Pd nanoparticles.

Finally, it is important to discuss also the possible implications of our observed trends on the magnetization measurements of Taniyama *et al.*[18] and Guzman and co-workers[19] performed on Fe-dilute Fe-Pd nanoparticles. In both works it has been found that when decreasing the particle size for a fixed composition, a reduction in the saturation magnetization per atom is obtained. These experimental measurements are very interesting since they do not follow the expected trend in which, when decreasing the size of magnetic nanoparticles, an increase in the average magnetization is always obtained due to the reduction in the average coordination number. However, both groups have offered different explanations of their results. On the one hand, Taniyama *et al.* state that this reduction can be understood by assuming the existence of a nonmagnetic surface shell, having a well-defined thickness, together with a core region having a saturation magnetization enhanced (by a factor of 1.3) when compared to that of the bulk Fe-Pd alloy. On the other hand, Guzman and co-workers argue that, since no oxide phase was observed in their x-ray diffraction patterns, the origin of the measured data could be explained if it is assumed that, in the nanoparticles, the polarization of the 4*d* palladium electrons by the iron impurities is not very effective. Interestingly, from our results shown in Fig. 12(a), we can see that both scenarios can occur in our considered Fe-Pd nanoparticles, without invoking any oxygen chemisorption on the surface, for well-defined types of chemical order. We can see [Fig. 12(a)] that, if the Fe species are mainly located in the core region (dashed line), relatively large local magnetization values are found for the Pd atoms near the center of the particles, $\sim 0.5\mu_B$/atom, together with a weakly polarized surface region. On the contrary, if the magnetic impurities are placed in the outermost shells (continuous line), we can appreciate that a less effective polarization of the Pd host is obtained, characterized by values of $2S(j)$ of $\sim 0.1\mu_B$/atom and the existence of antiferromagnetic arrays. In contrast, in the more homogeneously alloyed configuration, both the core and surface regions have a well-defined local magnetization that varies in the range of $\sim 0.4-0.6\mu_B$/atom. Even if our results are not strictly comparable to both experimental works, we believe that the microscopic features presented in this paper could help to shed some more light onto the understanding of the measured data.

V. SUMMARY AND CONCLUSIONS

In this work, we have systematically studied the chemical order and magnetic properties of Fe-dilute Fe-Pd nanoparticles by using a many-body semiempirical potential derived in the framework of the generalized second moment approximation and tight-binding self-consistent electronic structure calculations, respectively. We have found that significant variations in the composition and chemical order can have an important effect on the magnetic properties of Fe-Pd cluster alloys. The interaction of Fe impurities with the Pd atoms of the particles results in strong variations in the magnetic response at the host atoms surrounding the Fe sites, leading to the formation of magnetic nanoparticles with a very inhomogeneous local moment distribution. The extension and magnetic structure of the Fe-induced polarization cloud has been compared with those obtained for a single Fe impurity in bulk Pd calculated using the same model. It strongly depends on the size and surface termination of the particles, as well as on the precise location and number of the iron impurities in the structures, and can lead to sizable quenchings or enhancements of the average magnetization. Interestingly, we have found that the lowest energy atomic arrangements are always obtained when the Fe impurities accumulate in the subsurface region of the particles showing a very strong tendency to separate, a result that could be important in order to improve the catalytic properties of nanometer-sized palladium structures. Finally, we show that the value of the orbital-to-spin ratio in our Fe-Pd clusters is very sensitive to the changes in the internal position of the Fe impurities in the Pd particles; a result that suggests that x-ray magnetic circular dichroism experiments can be very useful in order to reveal well-defined features of the chemical order in these magnetic nanoparticles.

ACKNOWLEDGMENTS

Two of us (M.C.D. and D.S.) acknowledge the kind hospitality of the Instituto de Física Manuel Sandoval Vallarta (San Luis Potosí) where part of this work was done. R.A.G.-L. would like to acknowledge the kind hospitality of the CEA (Saclay) and to CONACyT (Mexico) for financial support under Project No. 45928-F.

*Electronic address: guirado@ifisica.uaslp.mx
†Electronic address: mcdjs@drecam.saclay.cea.fr
‡Electronic address: spanjaard@lps.u-psud.fr

[1] V. L. Moruzzi and P. M. Marcus, Phys. Rev. B **39**, 471 (1989).
[2] L. Fritsche, J. Noffke, and H. Eckardt, J. Phys. F: Met. Phys. **17**, 953 (1987).
[3] H. Chen, N. E. Brener, and J. Callaway, Phys. Rev. B **40**, 1443 (1989).
[4] A. J. Cox, J. G. Louderback, S. E. Apsel, and L. A. Bloomfield, Phys. Rev. B **49**, 12295 (1994); R. A. Guirado-López, D. Span-

jaard, and M. C. Desjonquères, *ibid.* **57**, 6305 (1998).
[5] G. G. Low and T. M. Holden, Proc. Phys. Soc. London **89**, 119 (1966).
[6] Q. Sun, Q. Wang, J. Z. Yu, Z. Q. Li, J. T. Wang, and Y. Kawazoe, J. Phys. I **7**, 1233 (1997).
[7] A. M. Clogston, B. T. Matthias, M. Peter, H. J. Williams, E. Corenzwit, and R. C. Sherwood, Phys. Rev. **125**, 541 (1962); P. A. Schroeder and C. Uher, Phys. Rev. B **18**, 3884 (1978) and references therein; J. F. van Acker, P. J. W. Weijs, J. C. Fuggle, K. Horn, H. Haak, and K. H. J. Buschow, *ibid.* **43**, 8903 (1991) and references therein.
[8] B. H. Verbeek, G. J. Nieuwenhuys, J. A. Mydosh, C. van Dijk, and B. D. Rainford, Phys. Rev. B **22**, 5426 (1980).
[9] O. Rader, C. Carbone, W. Clemens, E. Vescovo, S. Blügel, W. Eberhardt, and W. Gudat, Phys. Rev. B **45**, 13823 (1992); Z. Celinski, B. Heinrich, J. F. Cochran, W. B. Muir, A. S. Arrott, and J. Kirschner, Phys. Rev. Lett. **65**, 1156 (1990).
[10] S.-K. Lee, J.-S. Kim, B. Kim, Y. Cha, W. K. Han, H. G. Min, J. Seo, and S. C. Hong, Phys. Rev. B **65**, 014423 (2001).
[11] O. Rader, E. Vescovo, J. Redinger, S. Blugel, C. Carbone, W. Eberhardt, and W. Gudat, Phys. Rev. Lett. **72**, 2247 (1994); L. Cheng, Z. Altounian, D. H. Ryan, J. O. Strom-Olsen, M. Sutton, and Z. Tun, Phys. Rev. B **69**, 144403 (2004).
[12] C. A. Kuhnen and E. Z. da Silva, Phys. Rev. B **46**, 8915 (1992).
[13] H. Huang, J. Hermanson, J. G. Gay, R. Richter, and J. R. Smith, Surf. Sci. **172**, 363 (1986); D. Stoeffler, K. Ounadjela, J. Sticht, and F. Gautier, Phys. Rev. B **49**, 299 (1994); V. L. Moruzzi, P. M. Marcus, and S. L. Qiu, *ibid.* **52**, 3448 (1995); V. S. Stepanyuk, W. Hergert, K. Wildberger, R. Zeller, and P. H. Dederichs, *ibid.* **53**, 2121 (1996); L. Szunyogh, J. Zabloudil, A. Vernes, P. Weinberger, B. Újfalussy, and C. Sommers, *ibid.* **63**, 184408 (2001).
[14] A. Oswald, R. Zeller, and P. H. Dederichs, Phys. Rev. Lett. **56**, 1419 (1986).
[15] B. Delley, D. E. Ellis, and A. J. Freeman, J. Magn. Magn. Mater. **30**, 71 (1982).
[16] L. Yiping, G. C. Hadjipanayis, C. M. Sorensen, and K. J. Klabunde, J. Appl. Phys. **75**, 5885 (1994).
[17] K. Sato, B. Bian, and Y. Hirotsu, J. Appl. Phys. **91**, 8516 (2002).
[18] T. Taniyama, E. Ohta, T. Sato, and M. Takeda, Phys. Rev. B **55**, 977 (1997).
[19] M. Guzman, J. L. Delplancke, G. J. Long, J. Delwiche, M.-J. Hubin-Franskin, and F. Grandjean, J. Appl. Phys. **92**, 2634 (2002).
[20] R. Wunder and J. Phillips, J. Phys. Chem. **98**, 12329 (1994).
[21] J. Guevara, A. M. Llois, and M. Weissmann, Phys. Rev. B **52**, 11509 (1995).
[22] C. Barreteau, F. Raouafi, M. C. Desjonquères, and D. Spanjaard, Surf. Sci. **519**, 15 (2002).
[23] O. Fisher, M. Peter, and M. Steinemann, Helv. Phys. Acta **42**, 459 (1969); M. Methfessel, D. Hennig, and M. Scheffler, Phys. Rev. B **46**, 4816 (1992); L. Vitos, A. V. Ruban, H. L. Skriver, and J. Kollar, Surf. Sci. **411**, 186 (1998).
[24] G. M. Pastor, J. Dorantes-Dávila, and K. H. Bennemann, Phys. Rev. B **40**, 7642 (1989).
[25] R. Haydock, V. Heine, and M. J. Kelly, J. Phys. C **5**, 2845 (1972).
[26] V. Heine, Phys. Rev. **153**, 673 (1967).
[27] V. L. Moruzzi, J. F. Janak, and A. R. Williams, *Calculated Electronic Properties of Metals* (Pergamon, New York, 1978).
[28] P. Alvarado, J. Dorantes-Dávila, and G. M. Pastor, Phys. Rev. B **58**, 12216 (1998).
[29] M. Freyss, D. Stoeffler, and H. Dreyssé, Phys. Rev. B **56**, 6047 (1997).
[30] R. H. Victora, L. M. Falicov, and S. Ishida, Phys. Rev. B **30**, 3896 (1984).
[31] R. A. Guirado-López, M. C. Desjonquéres, and D. Spanjaard, Eur. Phys. J. D **36**, 67 (2005).
[32] V. Blum, Ch. Rath, S. Müller, L. Hammer, K. Heinz, J. M. García, J. E. Ortega, J. E. Prieto, O. S. Hernán, J. M. Gallego, A. L. Vázquez de Parga, and R. Miranda, Phys. Rev. B **59**, 15966 (1999).
[33] P. W. Murray, S. Thorshaug, I. Stensgaard, F. Besenbacher, E. Laegsgaard, A. V. Ruban, K. W. Jacobsen, G. Kopidakis, and H. L. Skriver, Phys. Rev. B **55**, 1380 (1997).
[34] K. S. Lee, S. H. Kim, H. G. Min, J. Seo, and J.-S. Kim, Surf. Sci. **377-379**, 918 (1997).
[35] W. Kim, W. Kim, S.-J. Oh, J. Seo, J.-S. Kim, H.-G. Min, and S. C. Hong, Phys. Rev. B **57**, 8823 (1998).
[36] J. R. Kitchin, J. K. Norskov, M. A. Barteau, and J. G. Chen, J. Chem. Phys. **120**, 10240 (2004).
[37] F. Baletto, C. Mottet, and R. Ferrando, Phys. Rev. Lett. **90**, 135504 (2003).
[38] X. Le Cann, C. Boeglin, B. Carriére, and K. Hricovini, Phys. Rev. B **54**, 373 (1996).
[39] J. Vogel, A. Fontaine, V. Cros, F. Petroff, J.-P. Kappler, G. Krill, A. Rogalev, and J. Goulon, Phys. Rev. B **55**, 3663 (1997).
[40] P. Kamp, A. Marty, B. Gilles, R. Hoffmann, S. Marchesini, M. Belakhovsky, C. Boeglin, H. A. Dürr, S. S. Dhesi, G. van der Laan, and A. Rogalev, Phys. Rev. B **59**, 1105 (1999).
[41] B. Sampedro, P. Crespo, A. Hernando, R. Litrán, J. C. Sánchez-López, C. López-Cartes, A. Fernandez, J. Ramírez, J. González-Calbet, and M. Vallet, Phys. Rev. Lett. **91**, 237203 (2003).
[42] T. Shinohara, T. Sato, and T. Taniyama, Phys. Rev. Lett. **91**, 197201 (2003).
[43] H. Bernas, J.-Ph. Attané, K.-H. Heinig, D. Halley, D. Ravelosona, A. Marty, P. Auric, C. Chappert, and Y. Samson, Phys. Rev. Lett. **91**, 077203 (2003).
[44] E. K. Parks, K. P. Kerns, and S. J. Riley, Chem. Phys. **262**, 151 (2000).
[45] H. Wende, A. Scherz, F. Wilhelm, and K. Baberschke, J. Phys.: Condens. Matter **15**, S547 (2003).
[46] M. Ulmeanu, C. Antoniak, U. Wiedwald, M. Farle, Z. Frait, and S. Sun, Phys. Rev. B **69**, 054417 (2004).
[47] G. M. Pastor, J. Dorantes-Dávila, S. Pick, and H. Dreyssé, Phys. Rev. Lett. **75**, 326 (1995); J. L. Rodríguez-López, J. Dorantes-Dávila, and G. M. Pastor, Phys. Rev. B **57**, 1040 (1998); R. Félix-Medina, J. Dorantes-Dávila, and G. M. Pastor, Phys. Rev. B **67**, 094430 (2003).
[48] M. B. Stearns, in 3*d,* 4*d, and* 5*d Elements, Alloys, and Compounds*, edited by H. P. J. Wijn, Landolt-Börnstein, New Series, Group 3, Vol. 19, Pt. a (Springer-Verlag, Berlin, 1986).